A SVM-Based Synchronized Fault Detection Method for 100% Renewable Microgrids

Preprint

Soham Chakraborty, Yue Chen, Ahmed Zamzam, and Jing Wang

National Renewable Energy Laboratory

Presented at the 50th Annual Conference of the IEEE Industrial Electronics Society (IECON)
Chicago, Illinois
November 3–6, 2024

NREL is a national laboratory of the U.S. Department of Energy
Office of Energy Efficiency & Renewable Energy
Operated by the Alliance for Sustainable Energy, LLC

This report is available at no cost from the National Renewable Energy Laboratory (NREL) at www.nrel.gov/publications.

Contract No. DE-AC36-08GO28308

Conference Paper
NREL/CP-5D00-87961
November 2024

A SVM-Based Synchronized Fault Detection Method for 100% Renewable Microgrids

Preprint

Soham Chakraborty, Yue Chen, Ahmed Zamzam, and Jing Wang

National Renewable Energy Laboratory

Suggested Citation
Chakraborty, Soham, Yue Chen, Ahmed Zamzam, and Jing Wang. 2024. *A SVM-Based Synchronized Fault Detection Method for 100% Renewable Microgrids: Preprint*. Golden, CO: National Renewable Energy Laboratory. NREL/CP-5D00-87961. https://www.nrel.gov/docs/fy25osti/87961.pdf.

NREL is a national laboratory of the U.S. Department of Energy
Office of Energy Efficiency & Renewable Energy
Operated by the Alliance for Sustainable Energy, LLC

This report is available at no cost from the National Renewable Energy Laboratory (NREL) at www.nrel.gov/publications.

Contract No. DE-AC36-08GO28308

Conference Paper
NREL/CP-5D00-87961
November 2024

National Renewable Energy Laboratory
15013 Denver West Parkway
Golden, CO 80401
303-275-3000 • www.nrel.gov

NOTICE

This work was authored in part by the National Renewable Energy Laboratory, operated by Alliance for Sustainable Energy, LLC, for the U.S. Department of Energy (DOE) under Contract No. DE-AC36-08GO28308. This work was supported by the Laboratory Directed Research and Development (LDRD) Program at NREL. The views expressed herein do not necessarily represent the views of the DOE or the U.S. Government.

Cover Photos by Dennis Schroeder: (clockwise, left to right) NREL 51934, NREL 45897, NREL 42160, NREL 45891, NREL 48097, NREL 46526.

SVM-Based Synchronized Fault Detection for 100% Renewable Microgrids

Soham Chakraborty, Yue Chen, Ahmed Zamzam, Jing Wang
Power Systems Engineering Center, National Renewable Energy Laboratory, Golden, Colorado 80401, USA
{soham.chakraborty, yue.chen, ahmed.zamzam, jing.wang}@nrel.gov

***Abstract*—Traditional protection schemes face significant challenges when applied to microgrids with high penetrations of renewables with inverter-based resources (IBRs). The proliferation of advanced sensing and communication technologies has generated copious data, offering an opportunity to overcome these limitations using data-driven machine learning approaches. This work proposes a novel approach based on a support vector machine (SVM) for detecting faults within a 100% renewable microgrid. The approach encompasses a systematic offline training stage for the development of a linear SVM-based fault detection algorithm. This process covers offline data collection from the microgrid under study, the extraction of features such as positive- and negative-sequence components and the total harmonic distortion of the voltage and current measurements of the relays, and the design of the linear SVM-based classifier. During the online implementation, however, different classifiers can exhibit asynchronicity in detecting the fault inception at different subcycle-to-cycle period-level delays. To circumvent this asynchronicity issue, a separate algorithm is developed for each relay to estimate the fault inception time as close to the real fault time. The performance of the proposed SVM-based synchronized fault detection method is evaluated using online time-domain simulation studies on a microgrid test system. The results corroborate the reliability of the fault detection scheme when tested under various fault cases (fault types, locations, and impedances) and non-fault cases during both grid-tied and islanded operation modes.**

I. Introduction

The design of a reliable protection system for microgrids has been a complex and pivotal issue for researchers both in industry and academia. The presence of distributed energy resources (DERs) introduces unique and dynamic behaviors in the event of a fault and commonly used protection schemes in distribution systems and microgrids face some challenges [1]. Several protection schemes have been proposed in the recent literature that include communication-assisted differential protection [2], adaptive directional overcurrent protection [3], sequence superimposed current-based overcurrent protection [4], admittance relay-based protection [5], and hybrid tripping characteristics-based protection [6]. These protection schemes provide a certain degree of reliability in protecting the microgrid with mixed DERs, including rotating machine-based DERs, such as diesel generation sets; gas turbine resources; and inverter-based resource (IBR) DERs, such as photovoltaic (PV) grid-following (GFL) IBRs and battery energy storage system (BESS) grid-forming (GFM) IBRs [7]. In the emerging 100% renewable microgrids, the additional challenges are:

- Low fault current contributions from the IBRs, constrained by semiconductor switches and current-limiter logic [8].
- Fault currents fluctuate based on IBRs' operational status, due to renewable resource variability [9].
- A lack of established fault models of IBRs, which can vary depending on the selection of the control schemes and the fault-limiting logic under balanced/unbalanced faults [10].

These challenges underscore the need for innovative fault detection methods, particularly in the context of 100% renewable microgrids, to ensure the reliability and effectiveness of the protection systems. With the advent of artificial intelligence techniques, the focus has shifted to using machine learning (ML) algorithms for developing more robust protection systems [11]. Decision tree (DT)-based algorithms for relays have been proposed using wavelet-based [12] and differential quantity-based [13] features; however, classical DT-based methods suffer from high variance and over-fitting issues. Multi-layer, feed-forward, artificial neural network-based algorithms have been developed based on instantaneous voltage and current measurements at relay points for fault classification and location identification [14], [15]; however, over-complexities due to a large number of neurons in the hidden layers and the impacts of limited, sparse, and noisy data affect the outcome. Other approaches include extreme ML and random forest algorithms, which use features extracted via Hilbert–Huang transformations and principal component analysis from measured voltage and current data [16], [17]. A threshold-based protection scheme based on Kalman filter residuals and the total harmonic distortion (THD) of measured current by the relays has been proposed in [18]. Support vector machine (SVM)-based classifiers have also been extensively used to detect and localize faults in a microgrid using unique features extracted from discrete wavelet transformation and discrete Fourier transformation of the prefault and postfault voltage and current measurements [19]–[23]. The main challenge in the existing SVM-based fault detection methods is that the classifiers (Kernels) are mostly nonlinear and are trained on post-computed features that are extremely difficult to implement in real low-cost, microcontroller-based numerical relays [24]. Despite their successful fault detection in microgrids with mixed DERs, most existing SVM classifier-based protection schemes are unable to detect faults under the intermittent behavior of renewable DERs [25]. This article fills the gap by contributing the following:

- A comprehensive and efficient approach to generating training data sets capturing the intermittency of renewable DERs, enabling the training of SVM classifiers that maintain reliability under varying levels of low-fault current situations within a 100% renewable microgrid.

This work was authored by the National Renewable Energy Laboratory (NREL), operated by Alliance for Sustainable Energy, LLC, for the U.S. Department of Energy (DOE) under Contract No. DE-AC36-08GO28308. This work was supported by the Laboratory Directed Research and Development (LDRD) Program at NREL. The views expressed in the article do not necessarily represent the views of the DOE or the U.S. Government. The U.S. Government retains and the publisher, by accepting the article for publication, acknowledges that the U.S. Government retains a nonexclusive, paid-up, irrevocable, worldwide license to publish or reproduce the published form of this work, or allow others to do so, for U.S. Government purposes.

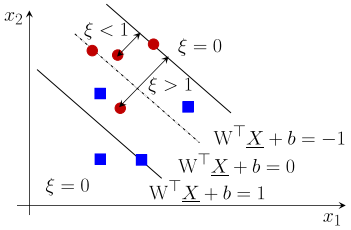

Fig. 1: Support vector machine-based maximum margin classifier.

• The utilization of classical features, such as positive- and negative-sequence components and the THD of the voltage and current waveforms measured by the relays, which facilitates the implementation on microcontroller-based relays.
• The development of a linear SVM classifier to detect faults, which can streamline integration into relay logic with fast detection speed and high accuracy.
• The introduction of a unique differential power-based fault time estimator, triggered by the SVM-based fault detector. This additional logic ensures synchronicity among multiple relays in a microgrid, which is crucial in any data-driven fault localization algorithm.

This article focuses on the development of an easy-to-implement and synchronized SVM-based fault detection method for a 100% renewable microgrid; the fault localization task is outside the scope of this article. The offline simulation results in the training stage showcase the reliability of the detection. The online simulation results on a 100% renewable microgrid corroborate the efficacy and viability of the implementation of the detection method.

II. Preliminaries of Support Vector Machine

SVM is a classification algorithm aiming to find the best hyperplane to separate data classes [26]. It maximizes the margin between closest data points (*support vectors*). It handles non-linear data via kernel functions like polynomial, radial basis function, or sigmoid kernels. SVM effectively handles high-dimensional data, even when features outnumber observations. For a two-class problem, the following linear kernel is commonly used:

$$y(\underline{X}) = \mathrm{W}^\top \underline{X} + b, \tag{1}$$

where $\underline{X}$ is the training set that includes N input vectors $\underline{X}_1, \underline{X}_2, \ldots, \underline{X}_\mathrm{N}$ and $\underline{X}_\mathrm{n} \in \mathbb{R}^\mathrm{P}$. The corresponding output targets are $t_1, t_2, \ldots, t_\mathrm{N}$ with $t_\mathrm{n} \in \{1, -1]\}$. $y(\underline{X})$ represents the model output that corresponds to the input data $\underline{X}$ and the classification is based on the sign of y(x). For instance, with $\underline{X}_\mathrm{n} \in \mathbb{R}^2$, as illustrated in Fig. 1. The red dots and blue squares represent the data samples for classes 1 and -1, respectively. It is common to observe that data samples from two classes may overlap as shown in Fig. 1. The SVM method introduces the margin, described as the minimum distance between the decision boundary and any of the samples. Define a slack variable as $\xi_\mathrm{n} = |t_\mathrm{n} - y(\underline{X}_\mathrm{n})|$. The classification of a dataset considering ξ_n can be written as $t_\mathrm{n} y(\underline{X}_\mathrm{n}) \geq 1 - \xi_\mathrm{n}$, $\mathrm{n} = 1, 2, \ldots, \mathrm{N}$. For the example in Fig. 1, if a red dot is located on the $\mathrm{W}^\top \underline{X}_\mathrm{n} + b = 1$ margin, then $\xi_\mathrm{n} = 0$. If a red dot is located between $\mathrm{W}^\top \underline{X}_\mathrm{n} + b = 0$ and $\mathrm{W}^\top \underline{X}_\mathrm{n} + b = 1$ margins, then $0 < \xi_\mathrm{n} < 1$. If a red dot is located on the $\mathrm{W}^\top \underline{X}_\mathrm{n} + b = 0$ margin, then $\xi = 1$. If a red dot is located between $\mathrm{W}^\top \underline{X}_\mathrm{n} + b = 0$ and $\mathrm{W}^\top \underline{X}_\mathrm{n} + b = -1$ margins, then $\xi > 1$. A similar pattern applies to the blue squares.

SVM aims to maximize the separating region between $\mathrm{W}^\top \underline{X}_\mathrm{n} + b = 1$ and $\mathrm{W}^\top \underline{X}_\mathrm{n} + b = -1$ margins as well as accounting for the mis-classified points through the slack parameters by minimizing the following optimization problem:

$$C \sum_{\mathrm{n}=1}^{\mathrm{N}} \xi_\mathrm{n} + \frac{1}{2} ||\mathrm{W}||^2, \tag{2}$$

where $C > 0$ provides a trade-off between the slack variables and the separating region. The Lagrangian is defined as

$$\begin{aligned} \mathcal{L}(\mathrm{W}, b, \mathrm{a}) =& C \sum_{\mathrm{n}=1}^{\mathrm{N}} \xi_\mathrm{n} + \frac{1}{2} ||\mathrm{W}||^2 - \sum_{\mathrm{n}=1}^{\mathrm{N}} \mu_\mathrm{n} \xi_\mathrm{n} \\ & - \sum_{\mathrm{n}=1}^{\mathrm{N}} \mathrm{a}_\mathrm{n} [t_\mathrm{n} (\mathrm{W}^\top \underline{X}_\mathrm{n} + b) - 1 + \xi_\mathrm{n}], \end{aligned} \tag{3}$$

where, $\mathrm{a}_\mathrm{n} > 0$ and $\mu_\mathrm{n} > 0$ are the Lagrange multipliers. Calculating the first derivative of eq. (3) with respect to W, b and ξ_n and making them equal to zero renders:

$$\mathrm{W} = \sum_{\mathrm{n}=1}^{\mathrm{N}} \mathrm{a}_\mathrm{n} t_\mathrm{n} \underline{X}_\mathrm{n}, \ \sum_{\mathrm{n}=1}^{\mathrm{N}} \mathrm{a}_\mathrm{n} t_\mathrm{n} = 0, \ \mathrm{a}_\mathrm{n} = C - \mu_\mathrm{n}. \tag{4}$$

Using eq. (4), eq. (3) can be reformulated as:

$$\begin{aligned} \mathcal{L}'(\mathrm{a}) = & \sum_{\mathrm{n}=1}^{\mathrm{N}} \mathrm{a}_\mathrm{n} - \frac{1}{2} \sum_{\mathrm{n}=1}^{\mathrm{N}} \sum_{\mathrm{m}=1}^{\mathrm{N}} \mathrm{a}_\mathrm{n} \mathrm{a}_\mathrm{m} t_\mathrm{n} t_\mathrm{m} \underline{X}_\mathrm{n}^\top \underline{X}_\mathrm{m}, \\ & 0 \leq \mathrm{a}_\mathrm{n} \leq C, \sum_{\mathrm{n}=1}^{\mathrm{N}} \mathrm{a}_\mathrm{n} t_\mathrm{n} = 0. \end{aligned} \tag{5}$$

From the optimization problem, the training points along with a_i form the *support vectors*, and optimal b are:

$$b = \frac{1}{\mathrm{N}_\mathcal{S}} \sum_{\mathrm{n} \in \mathcal{S}} [t_\mathrm{n} - \sum_{\mathrm{m} \in \mathcal{S}} \mathrm{a}_\mathrm{n} \mathrm{a}_\mathrm{m} \underline{X}_\mathrm{n} \underline{X}_\mathrm{m}], \tag{6}$$

where, $\mathrm{N}_\mathcal{S}$ is the total number of *support vectors*, that satisfy $t_\mathrm{n} y(\underline{X}_\mathrm{n}) = 1$ (i.e., they correspond to points that lie on the maximum margin hyper-planes).

III. Microgrid Model and Data Collection

To illustrate the data-driven approach, we consider the microgrid depicted in Fig. 2. This microgrid is based on Feeder 2 of the Banshee distribution benchmark system [27]. The original distribution network has one BESS (BESS 1), rated at 2.5 MVA, and one PV IBR (PV 1), rated at 2 MW, connected to Bus 1 and Bus 8, respectively. To convert the network into a 100% renewable microgrid, several additions have been made: BESS 2 with a rating of 1 MVA at Bus 9, PV 2 with a rating of 0.5 MW at Bus 6, and PV 3 with a rating of 1 MW at Bus 7. The BESS units are operating with GFM control, including power tracking for grid-connected mode and VF power sharing control for islanded mode. The PV units are operating in GFL control while following three modes: i) fixed power factor, ii) P-Q dispatch, and iii) volt-volt ampere reactive control. Both the BESS and the PV IBR systems respond to abnormal voltages and possess voltage ride-through capabilities compliant with IEEE 1547-2018 Category III [28]. More details about the ratings of the various buses, loads, and transformers can be found in [27]. In the data collection stage, the following steps are followed:
• **Step 1** The microgrid illustrated in Fig. 2 is simulated

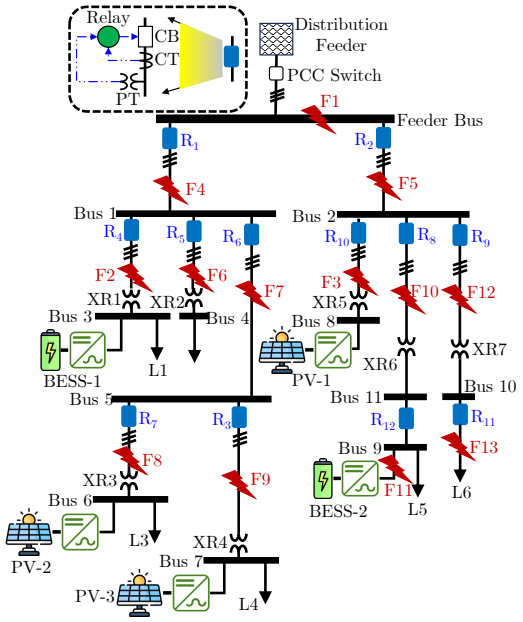

Fig. 2: The 100% renewable microgrid test system under study.

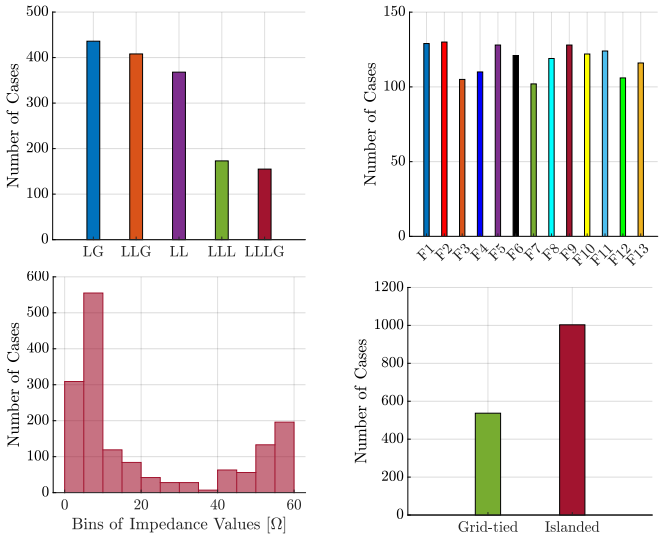

Fig. 3: Details of the 1,540 simulations in the offline data collection.

for a total of S times, covering both prefault and postfault situations. These simulations encompass a wide range of fault conditions, including different impedances, fault types, and fault locations. The simulations also account for variations in load demand; the solar irradiance of the PV IBRs; and different operational modes of IBRs, including both grid-tied and islanded configurations.

• **Step 2** All relay measurements, namely, $v_{\mathrm{a}}^{\mathrm{Rx}}(t)$, $v_{\mathrm{b}}^{\mathrm{Rx}}(t)$, $v_{\mathrm{c}}^{\mathrm{Rx}}(t)$, $i_{\mathrm{a}}^{\mathrm{Rx}}(t)$, $i_{\mathrm{b}}^{\mathrm{Rx}}(t)$, and $i_{\mathrm{c}}^{\mathrm{Rx}}(t)$, measured by all relays in the microgrid are recorded and stored.

In this study, a total of 1,540 fault simulations are conducted covering varying fault impedances, types, and locations. An overview of the types of simulations is shown in Fig. 3.

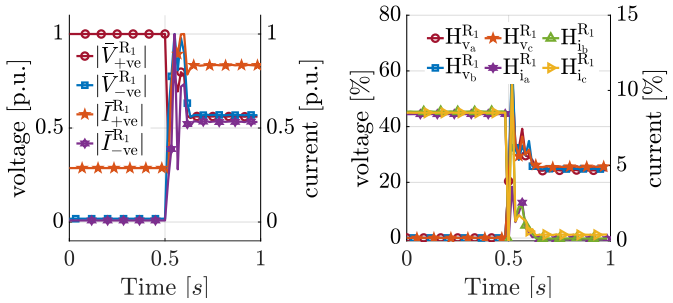

Fig. 4: The features computed by relay R_1 for fault F1 of type BCG with impedance of 1.4 Ω at $t = 0.5s$ in the microgrid of Fig. 2.

IV. Proposed SVM-Based Protection Design

In this section, the offline training of the SVM-based classifier is designed based on the collected data mentioned in Section III. The design phase consists of two main technical components: "Design of SVM-Based Fault Detection Classifier" and "Design of Fault Time Estimator."

A. Design of SVM-Based Fault Detection Classifier

The fault detection algorithm consists of two functionalities: feature extraction and fault classification.

1) Feature Extraction

Various types of faults in a microgrid generate various types of signatures/features in the waveform of the voltage and current measured by the relays. In this work, the following features are considered:

• **Sequence Components of Voltage**: The magnitudes of positive- and negative-sequence components of voltages are:

$$|\bar{V}_{+\mathrm{ve}}^{\mathrm{Rx}}| := [\bar{V}_{\mathrm{a}}^{\mathrm{Rx}} + \alpha\bar{V}_{\mathrm{b}}^{\mathrm{Rx}} + \alpha^2\bar{V}_{\mathrm{c}}^{\mathrm{Rx}}]/3, \quad (7)$$

$$|\bar{V}_{-\mathrm{ve}}^{\mathrm{Rx}}| := [\bar{V}_{\mathrm{a}}^{\mathrm{Rx}} + \alpha^2\bar{V}_{\mathrm{b}}^{\mathrm{Rx}} + \alpha\bar{V}_{\mathrm{c}}^{\mathrm{Rx}}]/3, \quad (8)$$

where $\bar{V}_{\mathrm{a}}^{\mathrm{Rx}}$, $\bar{V}_{\mathrm{b}}^{\mathrm{Rx}}$, $\bar{V}_{\mathrm{c}}^{\mathrm{Rx}}$ are the phasor quantities corresponding to $v_{\mathrm{a}}^{\mathrm{Rx}}(t)$, $v_{\mathrm{b}}^{\mathrm{Rx}}(t)$, $v_{\mathrm{c}}^{\mathrm{Rx}}(t)$, respectively. Here, $\alpha := 1\angle 120°$.

• **Sequence Components of Current**: The magnitudes of positive- and negative-sequence components of the current are:

$$|\bar{I}_{+\mathrm{ve}}^{\mathrm{Rx}}| := [\bar{I}_{\mathrm{a}}^{\mathrm{Rx}} + \alpha\bar{I}_{\mathrm{b}}^{\mathrm{Rx}} + \alpha^2\bar{I}_{\mathrm{c}}^{\mathrm{Rx}}]/3, \quad (9)$$

$$|\bar{I}_{-\mathrm{ve}}^{\mathrm{Rx}}| := [\bar{I}_{\mathrm{a}}^{\mathrm{Rx}} + \alpha^2\bar{I}_{\mathrm{b}}^{\mathrm{Rx}} + \alpha\bar{I}_{\mathrm{c}}^{\mathrm{Rx}}]/3, \quad (10)$$

where $\bar{I}_{\mathrm{a}}^{\mathrm{Rx}}$, $\bar{I}_{\mathrm{b}}^{\mathrm{Rx}}$, $\bar{I}_{\mathrm{c}}^{\mathrm{Rx}}$ are the three-phase phasor quantities corresponding to $i_{\mathrm{a}}^{\mathrm{Rx}}(t)$, $i_{\mathrm{b}}^{\mathrm{Rx}}(t)$, $i_{\mathrm{c}}^{\mathrm{Rx}}(t)$, respectively.

• **THD of Voltage**: The THD of phase y of the voltage waveform is:

$$\mathrm{H}_{\mathrm{v_y}}^{\mathrm{Rx}} := \sqrt{\Big[\sum_{\mathrm{h}>1} |\bar{V}_{\mathrm{y,h}}^{\mathrm{Rx}}|^2\Big] / \Big[|\bar{V}_{\mathrm{y,1}}^{\mathrm{Rx}}|^2 + \sum_{\mathrm{h}>1} |\bar{V}_{\mathrm{y,h}}^{\mathrm{Rx}}|^2\Big]}, \quad (11)$$

where $|\bar{V}_{\mathrm{y,h}}^{\mathrm{Rx}}|$ is the magnitude of the h^{th} harmonic component of $v_{\mathrm{y}}^{\mathrm{Rx}}(t)$. As a result, $\mathrm{H}_{\mathrm{v_a}}^{\mathrm{Rx}}$, $\mathrm{H}_{\mathrm{v_b}}^{\mathrm{Rx}}$, $\mathrm{H}_{\mathrm{v_c}}^{\mathrm{Rx}}$ are the THD of the voltages in phase a, b, c, respectively.

• **THD of Current**: The THD of each phase of the current waveform is defined as:

$$\mathrm{H}_{\mathrm{i_y}}^{\mathrm{Rx}} := \sqrt{\Big[\sum_{\mathrm{h}>1} |\bar{I}_{\mathrm{y,h}}^{\mathrm{Rx}}|^2\Big] / \Big[|\bar{I}_{\mathrm{y,1}}^{\mathrm{Rx}}|^2 + \sum_{\mathrm{h}>1} |\bar{I}_{\mathrm{y,h}}^{\mathrm{Rx}}|^2\Big]}, \quad (12)$$

where $|\bar{I}_{\mathrm{y,h}}^{\mathrm{Rx}}|$ is the magnitude of the h^{th} harmonic component of $i_{\mathrm{y}}^{\mathrm{Rx}}(t)$. As a result, $\mathrm{H}_{\mathrm{i_a}}^{\mathrm{Rx}}$, $\mathrm{H}_{\mathrm{i_b}}^{\mathrm{Rx}}$, $\mathrm{H}_{\mathrm{i_c}}^{\mathrm{Rx}}$ are the THDs of the currents in phase a, b, c, respectively.

Fig. 4 and Fig. 5 show the change in the features computed

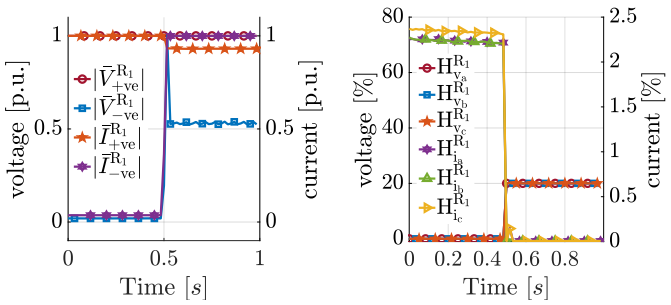

Fig. 5: The features computed by relay R_{12} for fault F10 of type AG with impedance of 10.1 Ω at $t = 0.5s$ in the microgrid of Fig. 2.

Algorithm 1: Algorithm for Fault Time Estimation

Input: Classifier's output [0 $\implies$ no-fault, 1 $\implies$ fault]
Output: $t_{\mathrm{f}}^{\mathrm{est}}$ in seconds
wait for classifier's output, $\mathcal{I}_{\mathrm{svm}}$.
if ($\mathcal{I}_{\mathrm{svm}} = 1$) **then**
use 1 cycle data of v_{a}, v_{b}, v_{c}, i_{a}, i_{b}, i_{c} from buffer
compute $\mathrm{d}P/\mathrm{d}t$, and $\mathrm{d}Q/\mathrm{d}t$
determine $t_{\mathrm{f}}^{\mathrm{est}}$ when $|\mathrm{d}P/\mathrm{d}t| > \tau$ OR $|\mathrm{d}Q/\mathrm{d}t| > \tau$
else if ($\mathcal{I}_{\mathrm{svm}} = 0$) **then**
no operation
end if
return $t_{\mathrm{f}}^{\mathrm{est}}$

by relay R_1 and R_{12} for fault F1 and F10 of type BCG and AG with impedances of 1.4 Ω and 10.1 Ω at $t = 0.5s$ in the microgrid of Fig. 2, respectively. As shown, there is a significant amount of change in the features before and after the fault inception. These observations justify the selection of these features for the classifier, which will be designed next. The complete set of the features for the relay Rx is:

$$\underline{X}_{\mathrm{feat}} := [|\bar{V}_{+\mathrm{ve}}^{\mathrm{Rx}}|\ |\bar{V}_{-\mathrm{ve}}^{\mathrm{Rx}}|\ |\bar{I}_{+\mathrm{ve}}^{\mathrm{Rx}}|\ |\bar{I}_{-\mathrm{ve}}^{\mathrm{Rx}}|\ \mathrm{H}_{\mathrm{v_a}}^{\mathrm{Rx}}\ \mathrm{H}_{\mathrm{v_b}}^{\mathrm{Rx}}\ \mathrm{H}_{\mathrm{v_c}}^{\mathrm{Rx}}\ \mathrm{H}_{\mathrm{i_a}}^{\mathrm{Rx}}\ \mathrm{H}_{\mathrm{i_b}}^{\mathrm{Rx}}\ \mathrm{H}_{\mathrm{i_c}}^{\mathrm{Rx}}]^{\top} \tag{13}$$

2) Fault Classification

The main focus of this section is to learn the SVM model offline using the training data set. The steps are:

- **Step 1**: From the stored data, as mentioned in Section III, we compute and define the set of features as discussed in Section IV-A1. In each simulation for the k^{th} relay, there are $\mathrm{n}_{\mathrm{pre}}$ number of $\underline{X}_{\mathrm{feat}}^{\mathrm{k}}$ and $\mathrm{n}_{\mathrm{post}}$ number of $\underline{X}_{\mathrm{feat}}^{\mathrm{k}}$ computed prefault and postfault, respectively; hence, there is a total of $\mathrm{N} = \mathrm{S} \times \mathrm{n}_{\mathrm{pre}} + \mathrm{S} \times \mathrm{n}_{\mathrm{post}}$ number of $\underline{X}_{\mathrm{feat}}^{\mathrm{k}}$ for the k^{th} relay.
- **Step 2**: The output target is selected such that $t_{\mathrm{n}} = -1$ and $t_{\mathrm{n}} = 1$ if $\underline{X}_{\mathrm{feat}}^{\mathrm{k}}[\mathrm{n}]$ belong to the prefault and postfault conditions, respectively. Based on the optimization method of Section II, the goal is to find the optimized linear classifier (a hyperplane of order 10) for the k^{th} relay.

We repeat these steps for all the relays. After determining the SVM classifier for each relay, in an ideal scenario, the classifier should categorize $\mathrm{S} \times \mathrm{n}_{\mathrm{post}}$ instances of $\underline{X}_{\mathrm{feat}}^{\mathrm{k}}$ as data from a system with a fault and $\mathrm{S} \times \mathrm{n}_{\mathrm{pre}}$ instances of $\underline{X}_{\mathrm{feat}}^{\mathrm{k}}$ as data from a system without a fault. This should be satisfied by all the relays associated with their respective SVM classifiers; however, the accuracy of the classification in the fault detection in practice might differ from the ideal case, which is discussed in Section V.

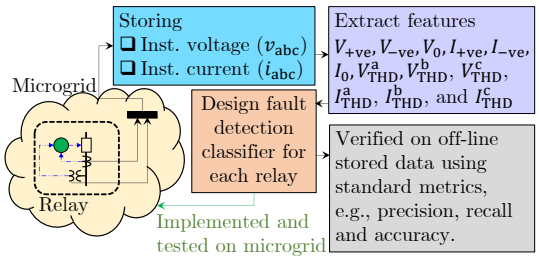

Fig. 6: Workflow of the proposed data-driven learning and scheme.

B. Design of Fault Time Estimator

The classifier detects the fault inception using the steady-state phasor quantities that causes a *subcycle*-to-*cycle* period-level delay in detection from the true fault inception time. And for the same fault inception time, different relays might detect the fault at different times. The delay in fault detection could result in the relay experiencing nuisance operations when coordinating with neighboring relays. To circumvent this asynchronicity issue, a separate algorithm is developed for each relay to estimate the fault inception time as close as possible to the real fault time. This algorithm requires using some instantaneous quantity, unlike the case of the fault detection classifier design. Here, the two candidates are the rate of change of active power, $\mathrm{d}P/\mathrm{d}t$ (in p.u./s), and the rate of change of reactive power, $\mathrm{d}Q/\mathrm{d}t$ (in p.u./s), measured at each relay. For relay Rx, the instantaneous active power and instantaneous reactive power in p.u. are formulated as:

$$P_{\mathrm{Rx}}(t) := \frac{v_{\mathrm{a}}^{\mathrm{Rx}}(t) i_{\mathrm{a}}^{\mathrm{Rx}}(t) + v_{\mathrm{b}}^{\mathrm{Rx}}(t) i_{\mathrm{b}}^{\mathrm{Rx}}(t) + v_{\mathrm{c}}^{\mathrm{Rx}}(t) i_{\mathrm{c}}^{\mathrm{Rx}}(t)}{S_{\mathrm{rated}}^{\mathrm{Rx}}},$$

$$Q_{\mathrm{Rx}}(t) := \frac{v_{\mathrm{bc}}^{\mathrm{Rx}}(t) i_{\mathrm{a}}^{\mathrm{Rx}}(t) + v_{\mathrm{ca}}^{\mathrm{Rx}}(t) i_{\mathrm{b}}^{\mathrm{Rx}}(t) + v_{\mathrm{ac}}^{\mathrm{Rx}}(t) i_{\mathrm{c}}^{\mathrm{Rx}}(t)}{\sqrt{3} \times S_{\mathrm{rated}}^{\mathrm{Rx}}},$$

where, $S_{\mathrm{rated}}^{\mathrm{Rx}}$ is the kVA rating of the line where the relay Rx is employed. Both the active and reactive power stay fairly constant before the fault under a specific loading and generation in the entire microgrid, and therefore the trajectory of $\mathrm{d}P(t)/\mathrm{d}t$ and $\mathrm{d}Q(t)/\mathrm{d}t$ will be fairly linear and the values will be close to zero; however, both quantities will drastically change their trajectory from the fault time. By observing the trajectories and checking the time instant when any of these two trajectories cross a preassigned upper and lower threshold limit, the fault time, $t_{\mathrm{f}}^{\mathrm{est}}$, can be estimated as close as possible to the true fault time, t_{f}. To avoid nuisance fault time estimation, this algorithm of threshold checking will be activated only when the detection algorithm successfully detects the fault. The fault time estimation algorithm will consider only the previous one cycle of the instantaneous voltage and current waveforms to compute $\mathrm{d}P(t)/\mathrm{d}t$ and $\mathrm{d}Q(t)/\mathrm{d}t$ for threshold checking. This is shown in Algorithm 1.

V. Results

The overall workflow of the proposed scheme is shown in Fig. 6. Firstly, the performance of the offline training of the SVM-based classifier in the fault detection is evaluated based on the $1,540$ fault scenarios, as mentioned in Section III. In this assessment, the presence of a fault is considered as the relevant element, and the confusion matrix is computed based on it with the true positive, false negative, false positive, and true negative to determine the metrics such as accuracy,

TABLE I: Performance of the SVM-based fault detection method on offline training data. Grtd = grid-tied, Isld = islanded.

Relay	Precision [%]		Recall [%]		Accuracy [%]	
	Grtd	Isld	Grtd	Isld	Grtd	Isld
R_1	97.44	97.31	95.07	96.03	94.63	95.01
R_2	97.89	97.22	95.12	96.52	94.58	95.12
R_3	97.13	97.72	94.96	96.11	94.79	94.97
R_4	97.25	97.11	95.07	95.96	94.88	94.87
R_5	97.69	97.43	95.11	96.03	94.66	95.06
R_6	97.56	97.63	95.26	96.05	94.37	95.12
R_7	97.81	97.56	94.93	96.11	94.33	95.21
R_8	97.52	97.87	95.33	96.16	94.38	95.30
R_9	97.22	97.19	95.03	95.91	94.23	94.98
R_{10}	97.88	97.37	95.18	95.96	94.99	95.11
R_{11}	97.44	97.79	95.01	96.11	95.12	95.13
R_{12}	97.51	97.27	94.93	95.02	95.17	95.18

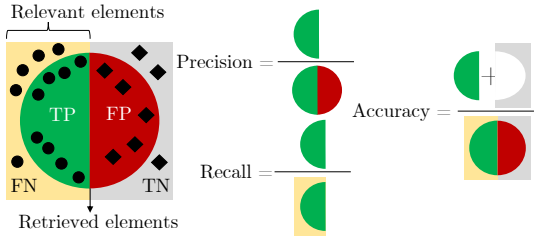

Fig. 7: Definition of precision, recall and accuracy (TP: True Positive, FN: False Negative, FP: False Positive, TN: True Negative).

precision, and recall. Table I shows the relay-wise performance of the offline-trained SVM classifier in detecting the fault. For instance, the precision across all the relays indicates that the SVM classifier is correct in predicting the fault approximately 97% to 98% of the time. The recall in all the relays concludes that the SVM classifiers find all cases of the fault with 94%–97% efficiency. The accuracy in all the relays concludes that approximately 94–96% of the time, the SVM classifier is correct in the fault classification overall. This corroborates the fact that the trained SVM-based classifier performs with high reliability in detecting faults. For instance, Fig. 8 and Fig. 9 show the instantaneous voltage and current waveform measured at relay R_2 under fault F1 of type BC with impedances 1.8 Ω during islanded mode and fault F10 of type CG with impedances 8.9 Ω during grid-tied mode, respectively. It is observed that during both the cases the proposed SVM-based classifier is successful in declaring the fault situation occurred at $t = 0.6$ s.

Moreover, the performance of the SVM-based fault detection and the fault time estimation algorithm is evaluated on new test scenarios. A MATLAB/Simulink-based time-domain simulation with a simulation time step of $T_s = 50\mu$ s of the microgrid shown in Fig. 2 with the proposed SVM-based fault detection scheme is conducted. In total, 750 cases are simulated covering various fault types, locations, impedances, and modes of microgrid operation. A relay-wise performance of the proposed SVM classifier with new datasets in run time is shown in Table II. The results illustrate that the SVM classifier-based fault detection method demonstrates a robust performance, characterized by high reliability exceeding 97%.

As mentioned in Section IV-B, once the fault detection block detects a fault, the fault estimation algorithm starts estimating the fault time based on the previous one cycle of data from the instance of detection. For instance, Fig. 10 and Fig. 11 show the performance of the fault time estimation

TABLE II: Performance of the fault detection method.

R_1	R_2	R_3	R_4	R_5	R_6
97.87%	97.73%	99.06%	99.06%	98.67%	99.06%
R_7	R_8	R_9	R_{10}	R_{11}	R_{12}
98.67%	99.33%	98.81%	98.93%	98.81%	99.06%

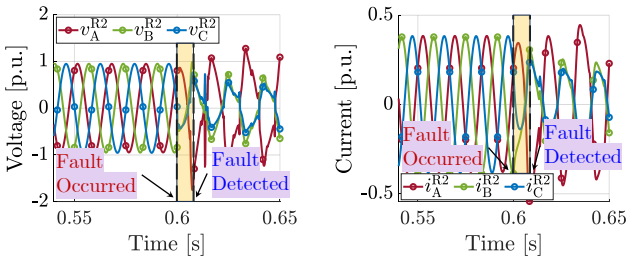

Fig. 8: Instantaneous voltage and current waveform measured at R_2 under fault F1 of type BC with impedances 1.8 Ω in islanded mode.

algorithm employed in relay R_2 under fault F1 and F10 of type BC and CG with impedances 1.8 Ω and 8.9 Ω, respectively. The fault occurred at $t_f = 0.6$ s, and the fault detection algorithm of relay R_2 detects at $t = 0.607$ s and $t = 0.61$ s, respectively. Based on Algorithm 1, R_2 estimate the fault time as $t_f^{est} = 0.6008$ s and $t_f^{est} = 0.6004s$, respectively; hence, it can be concluded that the fault time estimation algorithm, after activated by the fault detection scheme, estimates the time quite close to the real fault time. A relay-wise performance of the fault time estimation algorithm with the new datasets in run time is shown in Table III.

VI. Conclusion

This article proposes an SVM-based supervised machine learning algorithm for detecting faults by the relays employed in a 100% renewable microgrid. A systematic approach of the offline training stage for modeling a linear SVM-based fault detection algorithm is described covering the offline data collection stage-to-stage extraction of features, from the measurements of the relays to the design of the linear SVM-based classifier. Moreover, to circumvent the asynchronicity issue, a separate fault time estimation algorithm is developed for each relay before employing it in the online validation stage. The validation and results of the proposed SVM-based synchronized fault detection method using an online time-domain simulation study on a 100% renewable microgrid corroborate the enhanced reliability in detecting fault. While tackling the challenges of 100% renewable microgrid, the proposed SVM-based method with derivative of active and reactive power addresses the critical challenges of asynchronicity in detecting the timing of the exact fault occurrence and coordination between neighboring relays, which serves as the foundation of data-driven based protection. Comparative analysis of the proposed SVM-based protection system with traditional protection systems for such 100% renewable microgrid is considered as a important task for future.

References

[1] A. Hooshyar and R. Iravani, "Microgrid protection," *Proceedings of the IEEE*, vol. 105, no. 7, pp. 1332–1353, 2017.

[2] E. Sortomme, S. Venkata, and J. Mitra, "Microgrid protection using communication-assisted digital relays," *IEEE Transactions on Power Delivery*, vol. 25, no. 4, pp. 2789–2796, 2009.

[3] D. Lagos, V. Papaspiliotopoulos, G. Korres, and N. Hatziargyriou,

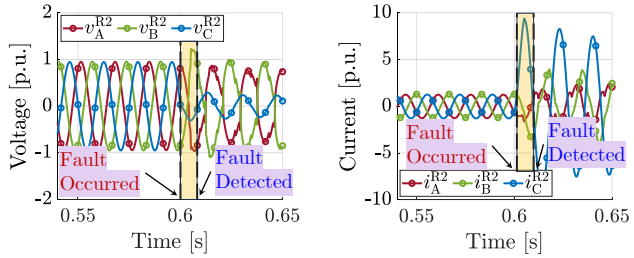

Fig. 9: Instantaneous voltage and current waveform measured at R_2 under fault F10 of type CG with impedances 8.9 Ω in grid-tied mode.

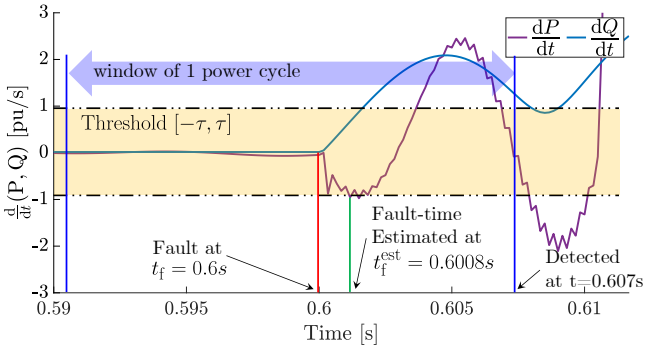

Fig. 10: The change of $\mathrm{d}P/\mathrm{d}t$, $\mathrm{d}Q/\mathrm{d}t$ at relay R_2 under fault F1 of type BC with impedances 1.8 Ω.

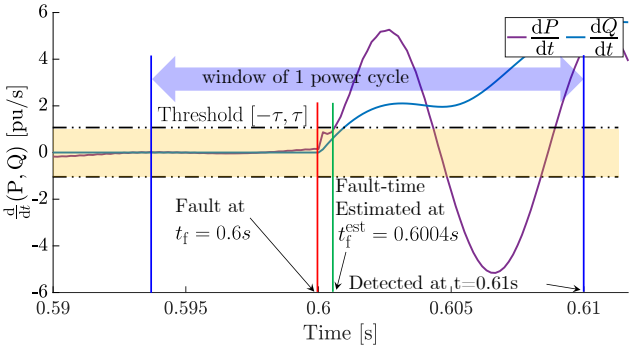

Fig. 11: The change of $\mathrm{d}P/\mathrm{d}t$, $\mathrm{d}Q/\mathrm{d}t$ at relay R_2 under fault F10 of type CG with impedances 8.9 Ω.

TABLE III: Performance of the fault time estimation algorithm.

Error [ms]	R_1	R_2	R_3	R_4	R_5	R_6
Max.	0.832	0.831	0.833	0.832	0.832	0.831
Min.	0.338	0.334	0.333	0.332	0.336	0.338
Error [ms]	R_7	R_8	R_9	R_{10}	R_{11}	R_{12}
Max.	0.833	0.833	0.832	0.831	0.831	0.832
Min.	0.339	0.333	0.335	0.337	0.336	0.331

"Microgrid protection against internal faults: Challenges in islanded and interconnected operation," *IEEE Power and Energy Magazine*, vol. 19, no. 3, pp. 20–35, 2021.

[4] M. A. Zamani, T. S. Sidhu, and A. Yazdani, "A protection strategy and microprocessor-based relay for low-voltage microgrids," *IEEE transactions on Power Delivery*, vol. 26, no. 3, pp. 1873–1883, 2011.

[5] M. Dewadasa, A. Ghosh, G. Ledwich, and M. Wishart, "Fault isolation in distributed generation connected distribution networks," *IET generation, transmission & distribution*, vol. 5, no. 10, pp. 1053–1061, 2011.

[6] S. Chakraborty and S. Das, "Communication-less protection scheme for ac microgrids using hybrid tripping characteristic," *Electric Power Systems Research*, vol. 187, p. 106453, 2020.

[7] W. M. Hamanah, M. I. Hossain, M. Shafiullah, and M. A. Abido, "Ac microgrid protection schemes: A comprehensive review," *IEEE Access*, vol. 11, pp. 76 842–76 868, 2023.

[8] J. Keller and B. Kroposki, "Understanding fault characteristics of inverter-based distributed energy resources," National Renewable Energy Lab.(NREL), Golden, CO (United States), Tech. Rep., 2010.

[9] Y. Zhao, B. Lehman, J.-F. de Palma, J. Mosesian, and R. Lyons, "Fault analysis in solar pv arrays under: Low irradiance conditions and reverse connections," in *2011 37th IEEE Photovoltaic Specialists Conference*, 2011, pp. 002 000–002 005.

[10] D. Ramasubramanian, P. Pourbeik, E. Farantatos, and A. Gaikwad, "Simulation of 100% inverter-based resource grids with positive sequence modeling," *IEEE Electrification Magazine*, vol. 9, no. 2, 2021.

[11] M. Uzair, L. Li, M. Eskandari, J. Hossain, and J. G. Zhu, "Challenges, advances and future trends in ac microgrid protection: With a focus on intelligent learning methods," *Renewable and Sustainable Energy Reviews*, vol. 178, p. 113228, 2023. [Online]. Available: https://www.sciencedirect.com/science/article/pii/S1364032123000849

[12] D. P. Mishra, S. R. Samantaray, and G. Joos, "A combined wavelet and data-mining based intelligent protection scheme for microgrid," *IEEE Transactions on Smart Grid*, vol. 7, no. 5, pp. 2295–2304, 2015.

[13] S. Kar, S. Samantaray, and M. D. Zadeh, "Data-mining model based intelligent differential microgrid protection scheme," *IEEE Systems Journal*, vol. 11, no. 2, pp. 1161–1169, 2015.

[14] M. U. Usman, J. Ospina, and M. O. Faruque, "Fault classification and location identification in a smart DN using ANN and AMI with real-time data," *The Journal of Engineering*, vol. 2020, no. 1, pp. 19–28, 2020.

[15] H. Lin, K. Sun, Z.-H. Tan, C. Liu, J. M. Guerrero, and J. C. Vasquez, "Adaptive protection combined with machine learning for microgrids," *IET generation, transmission & distribution*, vol. 13, no. 6, 2019.

[16] M. Mishra and P. K. Rout, "Detection and classification of micro-grid faults based on hht and machine learning techniques," *IET Generation, Transmission & Distribution*, vol. 12, no. 2, pp. 388–397, 2018.

[17] M. Uzair, M. E, L. Li, and J. Zhu, "Machine learning based protection scheme for low voltage ac microgrids," *Energies*, vol. 15, no. 24, 2022.

[18] F. Mumtaz, K. Imran, S. B. A. Bukhari, K. K. Mehmood, A. Abusorrah, M. A. Shah, and S. A. A. Kazmi, "A kalman filter-based protection strategy for microgrids," *IEEE Access*, vol. 10, pp. 73 243–73 256, 2022.

[19] M. Manohar, E. Koley, and S. Ghosh, "A reliable fault detection and classification scheme based on wavelet transform and ensemble of svm for microgrid protection," in *2017 3rd International Conference on Applied and Theoretical Computing and Communication Technology (iCATccT)*, 2017, pp. 24–28.

[20] B. Poudel, D. R. Garcia, A. Bidram, M. J. Reno, and A. Summers, "Circuit topology estimation in an adaptive protection system," in *2020 52nd North American Power Symposium (NAPS)*. IEEE, 2021, pp. 1–6.

[21] B. P. Poudel, A. Bidram, M. J. Reno, and A. Summers, "Zonal machine learning-based protection for distribution systems," *IEEE Access*, vol. 10, pp. 66 634–66 645, 2022.

[22] A. S. Zamzam and J. Wang, "Hierarchical data-driven protection for microgrids with 100% renewables," in *2023 IEEE Energy Conversion Congress and Exposition (ECCE)*, 2023, pp. 1506–1513.

[23] Y. Chen, A. S. Zamzam, S. Chakraborty, and J. Wang, "Decentralized microgrid protection through relative fault direction classification," in *2024 IEEE PES General Meeting (PESGM)*, 2024.

[24] V. V. Vijayachandran and U. J. Shenoy, "Implementation of support-vector-machine-based relay coordination scheme for distribution system with renewables," *IEEE Journal of Emerging and Selected Topics in Industrial Electronics*, vol. 2, no. 3, pp. 324–333, 2020.

[25] M. Manohar and E. Koley, "Svm based protection scheme for microgrid," in *2017 International Conference on Intelligent Computing, Instrumentation and Control Technologies*, 2017, pp. 429–432.

[26] C. M. Bishop and N. M. Nasrabadi, *Pattern recognition and machine learning*. Springer, 2006, vol. 4, no. 4.

[27] R. Salcedo, E. Corbett, C. Smith, E. Limpaecher, R. Rekha, J. Nowocin, G. Lauss, E. Fonkwe, M. Almeida, P. Gartner *et al.*, "Banshee distribution network benchmark and prototyping platform for hardware-in-the-loop integration of microgrid and device controllers," *The Journal of Engineering*, vol. 2019, no. 8, pp. 5365–5373, 2019.

[28] "IEEE standard for interconnection and interoperability of distributed energy resources with associated electric power systems interfaces," *IEEE Std 1547-2018*, pp. 1–138, 2018.